

Hyperfine structure of the metastable 3P_2 state of alkaline earth atoms as an accurate probe of nuclear magnetic octupole moments

K. Beloy and A. Derevianko

Physics Department, University of Nevada, Reno, Nevada 89557

W. R. Johnson

Physics Department, University of Notre Dame, Notre Dame, Indiana 46566

(Dated: November 9, 2018)

Measuring the hyperfine structure (HFS) of long-lived 3P_2 states of divalent atoms may offer the opportunity of extracting relatively unexplored nuclear magnetic octupole and electric hexadecapole moments. Here, using relativistic many-body methods of atomic structure and the nuclear shell model, we evaluate the effect of these higher nuclear moments on the hyperfine structure. We find that the sensitivity of HFS interval measurements in ^{87}Sr needed to reveal the perturbation caused by the nuclear octupole moment is on the order of kHz. Results of similar analyses for ^9Be , ^{25}Mg , and ^{43}Ca are also reported.

PACS numbers: 06.30.Ft, 32.10.Dk, 31.25.-v

I. INTRODUCTION

Progress in cooling and trapping techniques has enabled a number of advances in precision measurements of atomic properties. Compared to more traditional beam spectroscopy, trapping atoms or ions increases interrogation times and enhances spectral resolution. This is a well-recognized experimental trend spanning from the searches for permanent electric-dipole moments to atomic clocks. Here, we point out that measuring the hyperfine structure of long-lived 3P_2 states of cold divalent atoms may facilitate extracting the so far relatively unexplored nuclear magnetic octupole moments.

A nucleus may be described as a collection of electromagnetic moments. Generally, a nucleus of spin I possesses $2I$ moments beyond the monopole. Most well-known are the magnetic dipole (μ) and electric quadrupole (Q) moments. These two leading moments have been studied extensively and have contributed to the understanding of nuclear forces. For example, discovery of the quadrupole moment of the deuteron led to introducing nuclear tensor forces [1]. Here, we are interested in the next two moments in the multipolar hierarchy: nuclear magnetic octupole (Ω) and electric hexadecapole (Π) moments.

Electromagnetic fields of various nuclear moments perturb the motion of atomic electrons and reveal themselves in the hyperfine structure (HFS) of atomic and molecular levels. The resulting hyperfine intervals are conventionally parameterized in terms of the HFS constants A, B, C, D, \dots , each being proportional to the relevant nuclear multipolar moment. The perturbation becomes weaker as the rank of the multipole moment increases, and detecting the influence of higher multipole moments on the HFS intervals requires increasingly longer interrogation times. Also, to observe the effects of higher rank multipoles on the HFS structure one is forced to work with electronic states of relatively high angular momenta

J since the 2^k -pole moment only contributes in first order to the HFS structure of levels with $J \geq k/2$. These two factors have limited the determination of the octupole HFS constants to a small number of isotopes of Cl [2], Ga [3], Br [4], In [5], V [6], Eu [7], Lu [8], and Hf [9]. All of the above measurements have been carried out either on the ground state or on metastable states. The most recent octupole moment measurement was carried on the short-lived $6p_{3/2}$ state of ^{133}Cs [10]. Except for the case of the monovalent Cs atom, deducing octupole moments from measured HFS constants presents a formidable challenge, owing to the fact that the prerequisite atomic-structure calculations become inaccurate for multi-valent atoms. As a result, previous analyses focused primarily on *ratios* of octupole moments for various isotopes of the same atom, because the atomic-structure factor cancels out when ratios of HFS constants are formed. By contrast, the divalent alkaline-earth atoms considered here potentially yield direct values of the nuclear octupole moments.

3P_2 states in alkaline-earth atoms are well suited for extracting nuclear magnetic octupole moments. We list the relevant isotopes in Table I. The atomic lifetimes are longer than 100 seconds and are long enough to allow for a sufficiently high spectral resolution. Moreover, successful trapping of the 3P_2 alkaline-earth atoms Sr and Ca has been recently reported in a number of laboratories and there are ongoing efforts with Mg [13, 14, 15, 16]. A typical trapping time is longer than 10 seconds. Since the magnetic trap perturbs the atomic level structure, a plausible experiment could involve microwave spectroscopy of freely-falling atoms when trapping fields are turned off. Even then, the interrogation time is sufficiently long to permit a determination of the magnetic octupole HFS constant. To extract the nuclear octupole moment from the measured HFS constant, one requires electronic structure calculations. As shown in this paper, such supporting calculations can be carried out with an accuracy of a few per cent.

TABLE I: Nuclear parameters and lifetimes of the 3P_2 states of the stable isotopes of Be, Mg, Ca, and Sr. I is the nuclear spin; the superscript π represents the parity. Experimental dipole and quadrupole values are from Ref. [11]. Octupole and hexadecapole values are from a single-particle approximation (see Appendix A). Lifetimes for the 3P_2 states are from Ref. [12]

| Isotope | I^π | $\mu^{\text{exp.}} (\mu_N)$ | $Q^{\text{exp.}} (\text{b})$ | $\Omega^{\text{s.p.}} (\text{b} \times \mu_N)$ | $\Pi^{\text{s.p.}} (\text{b}^2)$ | 3P_2 Lifetime (s) |
|------------------|---------|-----------------------------|------------------------------|--|----------------------------------|----------------------|
| ^9Be | $3/2^-$ | $-1.177492(17)$ | $+0.053(3)$ | -0.073 | 0.00 | |
| ^{25}Mg | $5/2^+$ | $-0.85545(8)$ | $+0.201(3)$ | -0.15 | 0.00 | 1.06×10^3 |
| ^{43}Ca | $7/2^-$ | $-1.317643(7)$ | $-0.049(5)$ | -0.23 | 0.00 | 5.13×10^2 |
| ^{87}Sr | $9/2^+$ | $-1.0936030(13)$ | $+0.335(20)$ | -0.38 | 0.00 | 1.29×10^2 |

This paper is organized as follows. In Section II we recapitulate the major results from the relativistic theory of the hyperfine interaction. The consideration includes first-order effects of nuclear dipole, quadrupole, octupole, and hexadecapole moments and second-order dipole-dipole and dipole-quadrupole effects. In Section III, we focus on the electronic structure aspects of the problem and evaluate electronic coupling constants using a configuration-interaction (CI) method coupled with many-body perturbation theory (MBPT). We refer to this approximation as the CI+MBPT method. Further, in Section IV, we discuss our results for the HFS of the 3P_2 level in ^{87}Sr . Results for isotopes of Be, Mg, and Ca are tabulated in Appendix C. Finally, conclusions are drawn in Section V. The paper also has several appendices where we tabulate results of a technical nature. Unless specified otherwise, atomic units, $\hbar = |e| = m_e = 1$, and Gaussian electromagnetic units are employed throughout.

II. NUCLEAR MOMENTS AND THE HYPERFINE INTERACTION

The electric and vector potential of a nucleus modeled as a collection of point-like multipole moments may be expressed as

$$\begin{aligned} \varphi(\mathbf{r}) &= \sum_{k,\mu} (-1)^\mu \frac{1}{r^{k+1}} C_{k,\mu}(\hat{\mathbf{r}}) \mathcal{Q}_{k,-\mu}, \\ \mathbf{A}(\mathbf{r}) &= -i \sum_{k,\mu} (-1)^\mu \frac{1}{r^{k+1}} \sqrt{\frac{k+1}{k}} \mathbf{C}_{k,\mu}^{(0)}(\hat{\mathbf{r}}) \mathcal{M}_{k,-\mu}, \end{aligned} \quad (1)$$

where $C_{k,\mu}$ and $\mathbf{C}_{k,\mu}^{(0)}$ are normalized spherical harmonics and vector spherical harmonics, respectively (see, for example, Ref. [17]). In these expressions, $\mathcal{Q}_{k,\mu}$ and $\mathcal{M}_{k,\mu}$ are components of the nuclear electric and magnetic 2^k -pole (MJ and EJ) moment operators, respectively. Each of the moments is an irreducible tensor operator of rank k . Parity and time-reversal symmetries require that k is even for the electric moments and k is odd for the magnetic moments. Components of these tensors are conventionally parameterized using c-numbers that are defined as expectation values of the zero components of the operators in a nuclear stretched state $|I, M_I = I\rangle$. We will employ the following notation for the ‘‘stretched’’ matrix

element of a tensor operator $O_{k,\mu}$:

$$\langle O_k \rangle_I \equiv \langle I, M_I = I | O_{k,0} | I, M_I = I \rangle.$$

In particular, the magnetic-dipole, electric-quadrupole, magnetic-octupole, and electric-hexadecapole moments of the nucleus are defined as

$$\begin{aligned} \mu &= \langle \mathcal{M}_1 \rangle_I, \\ Q &= 2 \langle \mathcal{Q}_2 \rangle_I, \\ \Omega &= - \langle \mathcal{M}_3 \rangle_I, \\ \Pi &= \langle \mathcal{Q}_4 \rangle_I. \end{aligned}$$

The stretched matrix elements are related to the reduced matrix elements by

$$\langle I || O_k || I \rangle \equiv \begin{pmatrix} I & k & I \\ -I & 0 & I \end{pmatrix}^{-1} \langle O_k \rangle_I.$$

The interaction Hamiltonian for a single electron in an electromagnetic field is given by

$$h_{\text{em}}(\mathbf{r}) = \alpha \cdot \mathbf{A}(\mathbf{r}) - \varphi(\mathbf{r}),$$

and the total electromagnetic interaction Hamiltonian is then given by

$$H_{\text{em}} = \sum_i h_{\text{em}}(\mathbf{r}_i),$$

where the sum runs over all electron coordinates. Substituting the multipolar expansions (1) into the electromagnetic interaction Hamiltonian, we arrive at an expression for rotationally-invariant hyperfine-interaction (HFI) Hamiltonian in the form of

$$H_{\text{HFI}} = \sum_{k,\mu} (-1)^\mu T_{k,\mu}^e T_{k,-\mu}^n.$$

Here the spherical tensors (of rank k) $T_{k,\mu}^e$ act on electronic coordinates and $T_{k,\mu}^n$ operate in the nuclear space. We identify $T_{k,\mu}^n \equiv \mathcal{M}_{k,\mu}$ for odd k and $T_{k,\mu}^n \equiv \mathcal{Q}_{k,\mu}$ for even k . Explicitly, electronic tensors read

$$T_{k,\mu}^e = \sum_i t_{k,\mu}^e(\mathbf{r}_i),$$

with

$$t_{k,\mu}^e(\mathbf{r}) = \begin{cases} -\frac{1}{r^{k+1}} C_{k,\mu}(\hat{\mathbf{r}}) & \text{electric (even } k), \\ -\frac{i}{r^{k+1}} \sqrt{\frac{k+1}{k}} \alpha \cdot \mathbf{C}_{k,\mu}^{(0)}(\hat{\mathbf{r}}) & \text{magnetic (odd } k). \end{cases} \quad (2)$$

Matrix elements of these operators for Dirac bi-spinors are listed in Appendix B.

Now we recapitulate the application of perturbation theory to determining the hyperfine structure of atomic levels. In the presence of the multipolar fields produced by the nucleus, the total electronic angular momentum \mathbf{J} is no longer conserved. The conserved angular momentum includes the nuclear angular momentum \mathbf{I} ; explicitly this conserved angular momentum is $\mathbf{F} = \mathbf{I} + \mathbf{J}$. The proper basis consists of states $|\gamma I J F M_F\rangle$ generated by coupling nuclear and electronic wave functions,

$$|\gamma I J F M_F\rangle = \sum_{M_J, M_I} C_{JM_J; IM_I}^{FM_F} |\gamma J M_J\rangle |I M_I\rangle,$$

with γ encapsulating remaining electronic quantum numbers and the coupling coefficients being the conventional Clebsch-Gordon coefficients. For fixed values of J and I , the values of F range in $|J - I| \leq F \leq J + I$, implying that an unperturbed level with angular momentum J is split into $2J + 1$ levels for $J < I$ and into $2I + 1$ levels otherwise.

A matrix element of the HFI in the coupled basis is

$$\begin{aligned} \langle \gamma' I' J' F' M'_F | H_{\text{HFI}} | \gamma I J F M_F \rangle &= \delta_{F'F} \delta_{M'_F M_F} \\ \times (-1)^{I+J+F} \sum_k \begin{Bmatrix} F & J & I \\ k & I & J' \end{Bmatrix} \langle \gamma' J' || T_k^e || \gamma J \rangle \langle I || T_k^n || I \rangle, \end{aligned} \quad (3)$$

the δ -symbols reflecting the scalar character of the HFI in the coupled basis. Hyperfine corrections to an unperturbed level are given to first order by the diagonal matrix elements of H_{HFI} . For convenience, we write this correction in terms of the F -independent product of the stretched matrix elements

$$\begin{aligned} W_F^{(1)} &= \langle \gamma I J F M_F | H_{\text{HFI}} | \gamma I J F M_F \rangle \\ &= \sum_k X_k(I J F) \langle T_k^e \rangle_J \langle T_k^n \rangle_I, \end{aligned}$$

with

$$X_k(I J F) = (-1)^{I+J+F} \frac{\begin{Bmatrix} F & J & I \\ k & I & J \end{Bmatrix}}{\begin{pmatrix} J & k & J \\ -J & 0 & J \end{pmatrix} \begin{pmatrix} I & k & I \\ -I & 0 & I \end{pmatrix}}.$$

The first-order F -dependent effects are conventionally parameterized in terms of the hyperfine structure constants A, B, C, D, \dots . Successive labels correspond to contributions of a multipole of increasing multipolarity, e.g., A is due to the magnetic dipole moment, B due to the electric quadrupole moment, etc. The constants, up to D , are defined as in [18]:

$$\begin{aligned} A &= \frac{1}{IJ} \cdot \langle T_1^n \rangle_I \langle T_1^e \rangle_J = \frac{1}{IJ} \cdot \mu \langle T_1^e \rangle_J, \\ B &= 4 \cdot \langle T_2^n \rangle_I \langle T_2^e \rangle_J = 2 \cdot Q \langle T_2^e \rangle_J, \\ C &= \langle T_3^n \rangle_I \langle T_3^e \rangle_J = -\Omega \langle T_3^e \rangle_J, \\ D &= \langle T_4^n \rangle_I \langle T_4^e \rangle_J = \Pi \langle T_4^e \rangle_J. \end{aligned} \quad (4)$$

The second-order (in the HFI) correction for the state described by electronic quantum numbers γ and J is

$$W_F^{(2)} = \sum_{\gamma' J'} \frac{|\langle \gamma' I' J' F M_F | H_{\text{HFI}} | \gamma I J F M_F \rangle|^2}{E_{\gamma J} - E_{\gamma' J'}},$$

where the sum excludes the case $(\gamma' J') = (\gamma J)$. With Eq. (3) this can be expressed explicitly in terms of reduced matrix elements as

$$\begin{aligned} W_F^{(2)} &= \sum_{\gamma' J'} \frac{1}{E_{\gamma J} - E_{\gamma' J'}} \sum_{k_1, k_2} \begin{Bmatrix} F & J & I \\ k_1 & I & J' \end{Bmatrix} \begin{Bmatrix} F & J & I \\ k_2 & I & J' \end{Bmatrix} \\ &\times \langle \gamma' J' || T_{k_1}^e || \gamma J \rangle \langle \gamma' J' || T_{k_2}^e || \gamma J \rangle \langle I || T_{k_1}^n || I \rangle \langle I || T_{k_2}^n || I \rangle. \end{aligned}$$

For the case of interest, where $J = 2$, the sum over $(\gamma' J')$ is dominated by contributions from the adjacent fine structure levels ($\gamma 1$) and the sum over $k_1 k_2$ is dominated by the dipole-dipole ($k_1 = k_2 = 1$) term. If we limit ourselves to the dipole-dipole and dipole-quadrupole terms, then we may express the second-order correction as

$$\begin{aligned} W_F^{(2)} &= \left| \begin{Bmatrix} F & J & I \\ 1 & I & J-1 \end{Bmatrix} \right|^2 \eta \\ &+ \begin{Bmatrix} F & J & I \\ 1 & I & J-1 \end{Bmatrix} \begin{Bmatrix} F & J & I \\ 2 & I & J-1 \end{Bmatrix} \zeta \end{aligned}$$

where η and ζ are F -independent terms given by

$$\eta = \frac{(I+1)(2I+1)}{I} \mu^2 \frac{|\langle \gamma J-1 || T_1^e || \gamma J \rangle|^2}{E_{\gamma J} - E_{\gamma J-1}} \quad (5)$$

$$\begin{aligned} \zeta &= \frac{(I+1)(2I+1)}{I} \sqrt{\frac{2I+3}{2I-1}} \times \\ &\mu Q \frac{\langle \gamma J-1 || T_1^e || \gamma J \rangle \langle \gamma J-1 || T_2^e || \gamma J \rangle}{E_{\gamma J} - E_{\gamma J-1}} \end{aligned} \quad (6)$$

In the above expressions, γ denotes a given fine structure term such as 3P_2 and that $J' = J - 1 = 1$.

III. CI+MBPT ELECTRONIC WAVE FUNCTIONS

A precise analysis of the hyperfine structure depends on accurate electronic wave functions as well as nuclear multipole moments. To obtain accurate electronic wave functions, we used a combined method of configuration interaction (CI) and many-body perturbation theory (MBPT), which we refer to as CI+MBPT. The CI+MBPT method is described in detail, for example, in Refs. [19, 20]. Here, we restrict the presentation to a qualitative discussion and then apply the CI+MBPT method to determination of the HFS couplings.

The accuracy of the CI method is limited only by the completeness of the set of configurations used. In the context of CI+MBPT we refer to the sub-space containing the configurations to be treated by the CI method

as the model space. In CI+MBPT, additional contributions from configurations which are not in the model space can be accounted for by MBPT. For our purposes, we are interested in finding accurate wave functions. It is worth noting that the wave functions determined by the CI+MBPT analysis lie completely within the model space.

In deciding which configurations are to be included in the model space, we consider two things. First, configurations which interact strongly with the configuration of interest must be included in the model space. The main purpose here is to expand the model space to a degree in which the wave function can be described accurately. Second, configurations with energies which are nearly degenerate with the configuration of interest should also be included in the model space. These configurations lead to convergence problems in MBPT and are treated non-perturbatively by the CI method. Of course, “strongly” and “nearly degenerate” are relative terms which depend on the level of accuracy desired.

For the alkaline earth systems considered in this paper, we start with a lowest-order description of our system as two valence electrons outside a closed core in a central field. Configurations involving different excitations of the valence electrons outside the closed core tend to interact strongly and have relatively close energies. These configurations compose our model space. Additional contributions from configurations involving excitations from core electrons are then accounted for within the framework of MBPT.

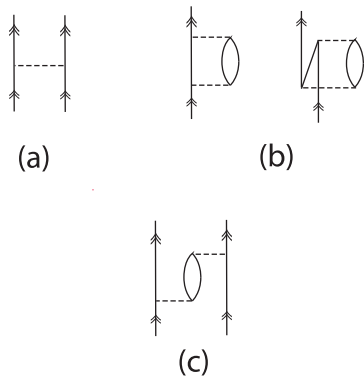


FIG. 1: Sample Brueckner-Goldstone diagrams included in the effective CI+MBPT Hamiltonian. (a) Coulomb interaction between the two valence electrons. The double-arrows indicate that the single-particle states originate/terminate in the model space. (b) Brueckner (core-polarization) diagrams. (c) Screening diagrams.

The relevant diagrams are shown in Fig. 1. The Coulomb interaction between the two valence electrons is taken into account essentially to all orders of perturbation theory and the remaining many-body effects (involving core excitations in the intermediate state) are treated in the second order of MBPT. In Fig. 1 the single-particle states are assumed to be generated in the frozen-core

TABLE II: Energies of Sr I obtained from CI+MBPT are compared to experimental values. The table is partitioned into states of definite J and parity. Energies are referenced from the ground $5s^2\ ^1S_0$ state. All energy values are in cm^{-1} .

| J | Parity | Level | CI+MBPT | Expt. | Diff. |
|-----|--------|---------------|---------|-------|-------|
| 0 | even | $5s6s\ ^1S_0$ | 30766 | 30592 | 174 |
| | | $5p^2\ ^3P_0$ | 35798 | 35193 | 605 |
| | | $5p^2\ ^1S_0$ | 37553 | 37160 | 393 |
| 1 | odd | $5s5p\ ^3P_1$ | 14841 | 14504 | 337 |
| | | $5s5p\ ^1P_1$ | 21818 | 21699 | 119 |
| | | $5s6p\ ^3P_1$ | 34062 | 33868 | 194 |
| | | $5s6p\ ^1P_1$ | 34293 | 34098 | 195 |
| 2 | odd | $5s5p\ ^3P_2$ | 15212 | 14899 | 313 |
| | | $4d5p\ ^3F_2$ | 33836 | 33267 | 569 |
| | | $4d5p\ ^1D_2$ | 34149 | 33827 | 322 |

(V^{N-2}) Dirac-Hartree-Fock (DHF) approximation where the so-called one-body (loop) diagrams vanish identically.

The specific approach that we used here is somewhat more sophisticated [20]: as the single-particle orbitals we employ the so-called Brueckner orbitals. This approach incorporates the diagrams Fig. 1(b) from the onset and also subsumes higher-order chains. Then the single-particle states (vertical lines) in the remaining diagrams are replaced by the Brueckner orbitals. The entire scheme incorporates all the second-order MBPT effects and includes certain classes of diagrams to all orders. Technically, generating Brueckner orbitals requires an energy-dependent self-energy operator (see, e.g., Ref. [20]), $\Sigma(\varepsilon_\kappa)$, which generally leads to non-orthogonal basis sets. We avoid this problem by fixing ε_κ to the V^{N-2} DHF energy of the lowest-energy valence orbital for a given angular symmetry κ (κ is defined explicitly in Appendix B).

To illustrate the predictive capabilities of the CI+MBPT method, in Table II we compare the theoretical energy values with the experimental values for Sr. The difference does not exceed a few $100\ \text{cm}^{-1}$ for all the calculated energy levels. While the accuracy can be improved further, this level is sufficient for the goals of the present paper.

Solving the CI+MBPT problem reduces to diagonalizing the effective Hamiltonian in the model space. With the CI+MBPT wave functions we proceed to evaluating matrix elements. Details are given in Ref. [20]; the method builds upon the formalism originally developed for He-like systems [21]. We also include an important chain of diagrams of the random-phase approximation (RPA) in the evaluation of matrix elements. Qualitatively, RPA accounts for screening of externally-applied fields (in our particular case these are the multipolar nuclear fields) by the core electrons.

Numerically, the calculations were carried out using B -spline basis sets. It is worth mentioning our modification to the original scheme [22] of generating the orbital sets.

In that scheme, boundary conditions are imposed on the small and large components of the wave function which were found to effectively dispense of spurious states in the orbital sets (more accurately, these spurious states were shifted towards the end of the spectrum). The disadvantage that follows is that the resulting wave functions are not highly accurate near the nucleus, leading to inaccuracies in the HFI integrals of Appendix B. To remedy this problem, we followed the prescription for creating a dual kinetic-balance (DKB) basis set, as introduced by Shabaev *et. al.* [23]. The DKB basis set is devoid of the problem of spurious states and capable of accurately representing the wave functions near the nucleus. The specific formulas used here for generating DHF orbital sets with a DKB basis set derived from B -splines are presented in Ref. [24].

Another technical issue is the appearance of “intruder” states in screening diagrams, Fig. 1(c). Intermediate states (the diagram is cut across horizontally) there involve core-excited states. Since our model (CI) space is essentially complete, such core-excited states become embedded in the two-particle energy spectrum of the lowest-order model Hamiltonian. This leads to singular energy denominators in the diagrams Fig. 1(c). We remedied this problem by evaluating screening corrections only to the two particle states that had energies below the lowest-energy core excitation. For a typical basis set the resulting subspace involved roughly 10% of the entire model space. Arguably, this prescription recovers most of the relevant correction since this low-energy subspace contains the dominant configurations.

IV. HYPERFINE STRUCTURE OF ^{87}Sr

Using the techniques described in the previous sections, we consider as a specific example the hyperfine structure of the lowest-energy 3P_2 level of ^{87}Sr .

A. Extracting the magnetic-octupole constant from measurement of hyperfine intervals

The nuclear spin of the stable ^{87}Sr isotope is $I = 9/2$, and so there are five hyperfine structure levels $F = 5/2, \dots, 13/2$. First-order corrections are then characterized by four hyperfine structure constants A, B, C , and D . In addition, the second-order dipole-dipole interaction, characterized by η and the dipole-quadrupole interaction, characterized by ζ , mix the 3P_2 state with the nearby fine structure 3P_1 state. Using the expressions given in Section II, we may write the hyperfine correc-

tion for ^{87}Sr in terms of these constants as

$$\begin{aligned} W_{5/2} &= -11A + \frac{11}{24}B - \frac{143}{42}C + \frac{143}{18}D, \\ W_{7/2} &= -\frac{15}{2}A + \frac{1}{48}B + \frac{65}{21}C - \frac{52}{3}D \\ &\quad + \frac{7\eta}{900} - \frac{7\zeta}{300\sqrt{6}}, \\ W_{9/2} &= -3A - \frac{7}{24}B + \frac{13}{6}C + \frac{91}{6}D \\ &\quad + \frac{32\eta}{2475} - \frac{4\zeta}{825}\sqrt{\frac{2}{3}}, \\ W_{11/2} &= \frac{5}{2}A - \frac{7}{24}B - \frac{10}{3}C - \frac{56}{9}D \\ &\quad + \frac{13\eta}{1100} + \frac{13\zeta}{550\sqrt{6}}, \\ W_{13/2} &= 9A + \frac{1}{4}B + C + D. \end{aligned}$$

The resulting HFS intervals $\delta W_F = W_F - W_{F+1}$ are given in terms of the hyperfine constants as

$$\begin{aligned} \delta W_{5/2} &= -\frac{7}{2}A + \frac{7}{16}B - \frac{13}{2}C + \frac{455}{18}D \\ &\quad - \frac{7\eta}{900} + \frac{7\zeta}{300\sqrt{6}}, \\ \delta W_{7/2} &= -\frac{9}{2}A + \frac{5}{16}B + \frac{13}{14}C - \frac{65}{2}D \\ &\quad - \frac{17\eta}{3300} - \frac{\zeta}{220}\sqrt{\frac{3}{2}}, \\ \delta W_{9/2} &= -\frac{11}{2}A + \frac{11}{2}C + \frac{385}{18}D \\ &\quad + \frac{\eta}{900} - \frac{\zeta}{30\sqrt{6}}, \\ \delta W_{11/2} &= -\frac{13}{2}A - \frac{13}{24}B - \frac{13}{3}C - \frac{65}{9}D \\ &\quad + \frac{13\eta}{1100} + \frac{13\zeta}{550\sqrt{6}}. \quad (7) \end{aligned}$$

Similar expressions for the hyperfine intervals in 3P_2 states of stable isotopes of other alkaline-earth atoms are given in Appendix C. Solving Eqs.(7) for the hyperfine constants C and D , one finds

$$\begin{aligned} C &= -\frac{3}{50}\delta W_{5/2} + \frac{7}{550}\delta W_{7/2} \\ &\quad + \frac{21}{275}\delta W_{9/2} - \frac{147}{3575}\delta W_{11/2} + \frac{7\zeta}{1375\sqrt{6}} \quad (8) \\ D &= \frac{3}{350}\delta W_{5/2} - \frac{9}{550}\delta W_{7/2} \\ &\quad + \frac{3}{275}\delta W_{9/2} - \frac{9}{3575}\delta W_{11/2} \quad (9) \end{aligned}$$

Expressions for the HFS constants C and D in terms of hyperfine intervals for 3P_2 states in other isotopes of the alkaline-earth atoms are given in Appendix C. The

constant C depends only on the second-order dipole-quadrupole interference term ζ while D is independent of both η and ζ . This proposition is independent of nuclear spin I , as shown in Appendix D.

To reiterate, measuring hyperfine intervals of the 3P_2 level should allow one to deduce the magnetic-octupole HFS constant C , limited only by the knowledge of ζ . With the aid of calculations of the electronic structure factor presented below one may extract the nuclear magnetic octupole moment of interest.

B. Electronic structure factors

From Eqs. (4) and (5) we see that the HFS constants may be written in terms of products of electronic matrix elements and nuclear multipole moments. We evaluate the electronic matrix elements using the relativistic many-body method described in Section III. We present the results of our calculations at various levels of approximation in Table III.

In generating the DHF orbitals we included nuclear-size effects by assuming a Fermi charge distribution inside the nucleus. For computation of HFI integrals, however, we assumed a point-size nucleus. The observed effect on the choice of a particular model of nuclear distribution is below our theoretical error for solving the electronic-structure problem.

There are several observations to be made with respect to the many-body calculations. First of all, we find that for Sr, the configuration $5p_{3/2}5s_{1/2}$ provides the dominant (92%) contribution to the CI wave function of the 3P_2 state. In particular, due to the angular selection rules, the constants B and C are determined by the matrix elements involving the $5p_{3/2}$ orbital from this dominant configuration. By contrast, the dominant $5p_{3/2}5s_{1/2}$ configuration does not contribute to the electric-hexadecapole (E4) constant due to selection rules for single-particle matrix elements (see Appendix). Therefore the E4 electronic factor is strongly suppressed, as its value is accumulated entirely due to admixed configurations.

We find that the BO (core-polarization) corrections universally increase the absolute value of all the constants. Qualitatively, core polarization describes an attraction of the valence electron by the core. This attraction leads to enhanced density closer to the nucleus and simultaneously larger hyperfine constants. Similarly, the computed RPA corrections show that the internal nuclear fields are enhanced by virtual core excitations. The screening diagrams, Fig. 1(c), qualitatively represent an effect of “cross-talking” between electrons via core polarization: a valence electron polarizes the core and this induced polarization attracts or repels another valence electron. We see for the magnetic-dipole HFS constant that this effect is relatively weak compared to the other many-body corrections; however, its effect is more substantial for the electric-quadrupole and magnetic-octupole HFS

constants. In all three of these cases, the screening contribution has the effect of decreasing the absolute value of the HFS constants.

Finally, in Table III we compare our *ab initio* results with experimental values for A and B . We find an 8% agreement for both constants. We believe that these accuracies are indicative of the theoretical error for the electronic factor entering the magnetic-octupole constant C . The accuracy of computing the electronic factor for the HFS constant D is expected to be worse because the entire value is accumulated due to correlation effects.

We have carried out similar many-body calculations for the parameters η and ζ entering the second-order correction to the hyperfine constants. For ^{87}Sr , we find $\eta = 6.65$ MHz and $\zeta = 0.529$ MHz. These second-order corrections are scaled to the experimental A and B coefficients and are accurate to 2%. The second-order dipole-quadrupole contribution to C is

$$\Delta C(^{87}\text{Sr}) = \frac{7\zeta}{1375\sqrt{6}} = 1.10(2) \text{ kHz}. \quad (10)$$

In this section we have described our calculations for ^{87}Sr . The corresponding results for ^9Be , ^{25}Mg , and ^{43}Ca are given in Appendix C.

V. DISCUSSION

At this point we combine the computed electronic structure factors for the magnetic-octupole constants (Table III and Table IV) and the nuclear shell-model prediction for the M3 moment Ω (Table I and Appendix A). We find that

$$\begin{aligned} C(^9\text{Be}) &= -3.57 \times 10^{-2} \text{ Hz}, \\ C(^{25}\text{Mg}) &= -2.57 \text{ Hz}, \\ C(^{43}\text{Ca}) &= -16.2 \text{ Hz}, \\ C(^{87}\text{Sr}) &= -201 \text{ Hz}. \end{aligned} \quad (11)$$

In particular for Sr, using Eq.(8), we may deduce that an experimental sensitivity in measuring the HFS intervals on the order of $\sigma_{\delta W} \approx 1$ kHz would result in an uncertainty in the C constant on the order of $\sigma_C \approx 0.11 \sigma_{\delta W} \approx 100$ Hz and would thus be capable of revealing the effects of a C constant of the predicted magnitude.

The expression for the constant of interest C in term of HFS splittings contains the second-order dipole-quadrupole correction, see, e.g., Eq.(8) for Sr. If the experiment measures HFS intervals with a vanishingly small error bar, the extraction of Ω would be limited by the error in this correction. Our estimated error bar for Sr, Eq. (10) is 20 Hz, which translated into 10% error bar for $C(^{87}\text{Sr})$ of predicted magnitude. Similar conclusion holds for Ca, while for Mg our estimated uncertainty in the dipole-quadrupole correction is comparable with the predicted size of C . For Be, our present uncertainty of 0.2 Hz in the dipole-quadrupole correction precludes

TABLE III: Breakdown of many-body corrections to hyperfine structure constants of $^{87}\text{Sr } 5s5p^3P_2$ state. We used $\mu = -1.0936\mu_N$ and $Q = 0.305(2)$ b (Ref. [25]) in tabulating A and B constants. The final result is compared with experimental values from Ref. [26]. CI-DHF corresponds to CI values computed using single-particle basis generated in the frozen-core (V^{N-2}) DHF potential.

| | A , MHz | B , MHz | C/Ω , MHz/ $(\mu_N \times \text{b})$ | D/Π , MHz/b ² |
|-----------------|-------------|------------|---|------------------------------|
| CI-DHF | -147.1 | 35.6 | 3.54×10^{-4} | 0.54×10^{-12} |
| | | | Many-body corrections | |
| Δ BO | -41.9 | 10.2 | 1.03×10^{-4} | 0.85×10^{-12} |
| Δ Screen | 0.4 | -4.6 | -0.42×10^{-4} | 2.71×10^{-12} |
| Δ RPA | -42.0 | 21.0 | 1.15×10^{-4} | 0.55×10^{-12} |
| Final | -230.6 | 62.2 | 5.30×10^{-4} | 4.65×10^{-12} |
| Experiment | -212.765(1) | 67.215(15) | | |

clean extraction of the octupole moment. Notice, however, that the nuclear shell model estimates of the nuclear octupole moment may be unreliable. If the ^{133}Cs experiment [10] is of any indication, the “true” size of the octupole constant may be much larger (factor of 40) than predicted. Then the dipole-quadrupole corrections become mostly irrelevant.

We emphasize that the values (11) are only estimates based on the nuclear-shell model; measuring C would show deviations from these estimates. In a particular case of ^{133}Cs the measured and the predicted values differed by a factor of 40 [10]. It remains to be seen if such large deviations from the nuclear shell model would be revealed experimentally for the nuclei considered in the present work.

Acknowledgments

The work of KB and AD was supported in part by National Science Foundation grant No. PHY-06-53392 and the work of WRJ was supported in part by NSF grant No. PHY-04-56828.

APPENDIX A: NUCLEAR MOMENTS FROM A SINGLE PARTICLE MODEL

A crude approximation to the nuclear moments can be achieved by representing the nucleus by a single nucleon. For even-odd (even number of protons, odd number of neutrons) nuclei we use a single neutron, and for odd-even nuclei we use a single proton. Using formulas by Schwartz [27], we may write the moments in this single

particle model as

$$\begin{aligned}
 \mu^{\text{s.p.}} &= \mu_N I \times \begin{cases} [g_l + (g_s - g_l)/2I] & \text{for } I = l + \frac{1}{2}, \\ [g_l - (g_s - g_l)/(2I + 2)] & \text{for } I = l - \frac{1}{2}, \end{cases} \\
 Q^{\text{s.p.}} &= -e\langle r^2 \rangle g_l \frac{2I - 1}{2I + 2}, \\
 \Omega^{\text{s.p.}} &= \mu_N \langle r^2 \rangle \frac{3}{2} \frac{(2I - 1)}{(2I + 4)(2I + 2)} \\
 &\quad \times \begin{cases} (I + 2)[(I - \frac{3}{2})g_l + g_s] & \text{for } I = l + \frac{1}{2}, \\ (I - 1)[(I + \frac{5}{2})g_l - g_s] & \text{for } I = l - \frac{1}{2}, \end{cases} \\
 \Pi^{\text{s.p.}} &= -e\langle r^2 \rangle g_l \frac{3}{8} \frac{(2I - 1)(2I - 3)}{(2I + 4)(2I + 2)},
 \end{aligned}$$

where $g_l = +1$, $g_s = 5.58$ for a proton and $g_l = 0$, $g_s = -3.83$ for a neutron. All of the stable isotopes considered in this paper have even-odd nuclei. This has the immediate consequence $Q^{\text{s.p.}} = 0$ and $\Pi^{\text{s.p.}} = 0$ for all isotopes. Furthermore, an examination of the momentum I and parity π in Table I reveals that the nucleon for each isotope must have an orbital momentum l satisfying $I = l + 1/2$. With this additional consideration, $\mu^{\text{s.p.}} = -1.92\mu_N$ for all isotopes, and the expression for the octupole moment is reduced to

$$\Omega^{\text{s.p.}} = \mu_N \langle r^2 \rangle g_s \frac{3}{4} \frac{(2I - 1)}{(2I + 2)}.$$

Approximating the root-mean-square value of the nuclear radii, $\langle r^2 \rangle^{1/2}$, as (in units of fm) 2.52, 3.05, 3.48, and 4.24 for the cases of ^9Be , ^{25}Mg , ^{43}Ca , and ^{87}Sr , respectively, yields the values for $\Omega^{\text{s.p.}}$ given in Table I.

In the single particle model the electromagnetic moments of the nuclei are given by the appropriate expectation values for the valence nucleon shell. In this model the even-odd nuclei would have electromagnetic moments determined by the valence neutron. In particular, since the neutron doesn’t have an electric charge, all electric moments vanish. Certainly, the observed nonzero Q-moment provides an information on such quantities as nuclear deformation. Similarly, an observation of the electric hexadecapole moment, which is zero in the single particle approximation, should provide similar information on the nuclear distortion.

APPENDIX B: MATRIX ELEMENTS OF THE ELECTRONIC TENSOR OPERATOR

Here we compile expressions for the matrix elements of the single-particle electronic HFI coupling operators $t_{k,\mu}^e(\mathbf{r})$ given in Eq. (2). We use the conventional parametrization of the Dirac bi-spinors,

$$|n\kappa m\rangle = \frac{1}{r} \begin{pmatrix} iP_{n\kappa}(r) \Omega_{\kappa m}(\hat{r}) \\ Q_{n\kappa}(r) \Omega_{-\kappa m}(\hat{r}) \end{pmatrix},$$

where $\kappa = (l - j)(2j + 1)$ and Ω are spinor functions. With this parametrization, we find that the reduced matrix elements for the HFI couplings to electric moments of the nucleus are given by

$$\begin{aligned} \langle n'\kappa' || t_k^e || n\kappa \rangle &= -\langle \kappa' || C_k || \kappa \rangle \\ &\times \int_0^\infty \frac{dr}{r^{k+1}} (P_{n'\kappa'} P_{n\kappa} + Q_{n'\kappa'} Q_{n\kappa}), \end{aligned}$$

and for couplings to magnetic moments these are

$$\begin{aligned} \langle n'\kappa' || t_k^e || n\kappa \rangle &= \langle \kappa' || C_k || -\kappa \rangle \left(\frac{\kappa' + \kappa}{k} \right) \\ &\times \int_0^\infty \frac{dr}{r^{k+1}} (P_{n'\kappa'} Q_{n\kappa} + Q_{n'\kappa'} P_{n\kappa}). \end{aligned}$$

Selection rules for these matrix elements follow from those for the matrix elements of the C -tensor: $|j - j'| \leq k \leq j + j'$ and the sum $l + l'$ must be even.

APPENDIX C: HYPERFINE STRUCTURE OF THE 3P_2 STATE FOR ^9Be , ^{25}Mg , AND ^{43}Ca

This appendix contains a compilation of expressions relating the hyperfine intervals and the hyperfine structure constants for the 3P_2 states of ^9Be , ^{25}Mg , and ^{43}Ca . Computed HFS constants for these isotopes, given in Table IV, are also included.

^9Be , $I = 3/2$:

$$\begin{aligned} \delta W_{1/2} &= -\frac{3}{2}A + \frac{7}{8}B - 28C - \frac{11\eta}{600} + \frac{\sqrt{3}\zeta}{200}, \\ \delta W_{3/2} &= -\frac{5}{2}A + \frac{5}{8}B + 20C - \frac{\eta}{120} - \frac{\sqrt{3}\zeta}{40}, \\ \delta W_{5/2} &= -\frac{7}{2}A - \frac{7}{8}B - 7C + \frac{7\eta}{200} + \frac{7\zeta}{200\sqrt{3}}, \end{aligned}$$

$$C = -\frac{1}{50}\delta W_{1/2} + \frac{1}{50}\delta W_{3/2} - \frac{1}{175}\delta W_{5/2} + \frac{\zeta}{500\sqrt{3}}$$

For ^9Be , we find that $\eta = 25.09(4)$ MHz and $\zeta = 0.2939(2)$ MHz, leading to a value $\Delta C = 0.3394(2)$ kHz for the second-order correction to C .

^{25}Mg , $I = 5/2$:

$$\begin{aligned} \delta W_{1/2} &= -\frac{3}{2}A + \frac{9}{20}B - \frac{54}{5}C + 90D \\ &\quad - \frac{\eta}{100} + \frac{\zeta}{50\sqrt{2}}, \\ \delta W_{3/2} &= -\frac{5}{2}A + \frac{1}{2}B - 3C - 75D \\ &\quad - \frac{13\eta}{1260} - \frac{\zeta}{210\sqrt{2}}, \\ \delta W_{5/2} &= -\frac{7}{2}A + \frac{7}{40}B + \frac{49}{5}C + 35D \\ &\quad - \frac{\eta}{900} - \frac{11\zeta}{300\sqrt{2}}, \\ \delta W_{7/2} &= -\frac{9}{2}A - \frac{27}{40}B - \frac{27}{5}C - 9D \\ &\quad + \frac{3\eta}{140} + \frac{33\zeta}{140\sqrt{2}}. \end{aligned}$$

$$\begin{aligned} C &= -\frac{1}{30}\delta W_{1/2} - \frac{1}{70}\delta W_{3/2} + \frac{1}{20}\delta W_{5/2} \\ &\quad - \frac{5}{252}\delta W_{7/2} + \frac{\zeta}{350\sqrt{2}} \\ D &= \frac{1}{210}\delta W_{1/2} - \frac{3}{490}\delta W_{3/2} + \frac{3}{980}\delta W_{5/2} \\ &\quad - \frac{1}{1764}\delta W_{7/2} \end{aligned}$$

For ^{25}Mg , we find that $\eta = 5.37(1)$ MHz and $\zeta = 0.333(1)$ MHz, leading to a value $\Delta C = 0.671(2)$ kHz for the second-order correction to C .

^{43}Ca , $I = 7/2$:

$$\begin{aligned} \delta W_{3/2} &= -\frac{5}{2}A + \frac{25}{56}B - \frac{55}{7}C + \frac{275}{7}D \\ &\quad - \frac{\eta}{112} + \frac{\zeta}{112}\sqrt{\frac{5}{3}}, \\ \delta W_{5/2} &= -\frac{7}{2}A + \frac{3}{8}B - 44D \\ &\quad - \frac{\eta}{144} - \frac{\zeta}{48\sqrt{15}}, \\ \delta W_{7/2} &= -\frac{9}{2}A + \frac{3}{56}B + \frac{48}{7}C + \frac{180}{7}D \\ &\quad + \frac{\eta}{1680} - \frac{13\zeta}{560}\sqrt{\frac{3}{5}}, \\ \delta W_{9/2} &= -\frac{11}{2}A - \frac{33}{56}B - \frac{33}{7}C - \frac{55}{7}D \\ &\quad + \frac{11\eta}{720} + \frac{11\zeta}{240\sqrt{15}} \end{aligned}$$

$$C = -\frac{1}{20}\delta W_{3/2} + \frac{1}{15}\delta W_{7/2} - \frac{7}{220}\delta W_{9/2} + \frac{\zeta}{120\sqrt{15}}$$

$$D = \frac{1}{140}\delta W_{3/2} - \frac{1}{84}\delta W_{5/2} + \frac{1}{140}\delta W_{7/2} - \frac{1}{660}\delta W_{9/2}$$

For ^{43}Ca , we find that $\eta = 8.43(3)$ MHz and $\zeta = 0.085(1)$ MHz, leading to a value $\Delta C = -0.183(3)$ kHz for the second-order correction to C .

APPENDIX D: PROOF THAT HFS CONSTANTS C AND D MAY BE DEFINED COMPLETELY IN TERMS OF THE HFS INTERVALS

In this section we prove that the HFS constants C and D can be expressed uniquely in terms of the HFS intervals even when the second-order dipole-dipole fine structure term may not be neglected. This is a nontrivial statement, as the number of linear equations for HFS intervals is less than the number of fitting parameters. For example, for ^{87}Sr we find that there are four HFS intervals expressed in terms of five fitting parameters (see Eq.(7)).

We start by defining our HFS levels from a new energy offset, $W'_F = W_F + \Delta$. The constant Δ is arbitrary and its particular choice will be shown not to affect the conclusions; consequently, a knowledge of the HFS level intervals with a convenient choice of Δ is sufficient to completely define W'_F for all F . Including all first-order terms as well as the second-order dipole-dipole fine structure term, the levels W'_F can be written as

$$W'_F = \Delta + (-1)^{I+J+F} \sum_{k'} \left\{ \begin{matrix} F & J & I \\ k' & I & J \end{matrix} \right\} Z_{k'} + \left| \left\{ \begin{matrix} F & J & I \\ 1 & I & J-1 \end{matrix} \right\} \right|^2 \eta, \quad (\text{D1})$$

where $Z_k = \langle \gamma J || T_k^e || \gamma J \rangle \langle I || T_k^n || I \rangle$. From Eq. (4) we see that Z_1 is proportional to A , Z_2 is proportional to B , etc.. The next step is to multiply every term in Eq. (D1) by $(-1)^{I+J+F} (2F+1) \left\{ \begin{matrix} F & J & I \\ k & I & J \end{matrix} \right\}$, with $k \neq 0$, and sum over all F -values. Here we analyze the effect of this procedure on the individual terms of the right hand side of Eq. (D1); to do so, we incorporate various well-known sum rules of six- j symbols. The first term becomes

$$\Delta \cdot \sum_F (-1)^{I+J+F} (2F+1) \left\{ \begin{matrix} F & J & I \\ k & I & J \end{matrix} \right\} = \Delta \cdot \delta_{k,0} \sqrt{(2I+1)(2J+1)} = 0.$$

The second term becomes

$$\sum_{k'} Z_{k'} \sum_F (2F+1) \left\{ \begin{matrix} F & J & I \\ k' & I & J \end{matrix} \right\} \left\{ \begin{matrix} F & J & I \\ k & I & J \end{matrix} \right\} = \sum_{k'} Z_{k'} \frac{\delta_{k,k'}}{(2k+1)} = \frac{1}{(2k+1)} Z_k.$$

The third term becomes

$$\eta (-1)^{2(I+J)+k+1} \sum_F (-1)^{F-I-J-k-1} (2F+1) \times \left\{ \begin{matrix} F & J & I \\ 1 & I & J-1 \end{matrix} \right\} \left\{ \begin{matrix} F & J & I \\ 1 & I & J-1 \end{matrix} \right\} \left\{ \begin{matrix} F & J & I \\ k & I & J \end{matrix} \right\} = \eta (-1)^{2(I+J)+k+1} \left\{ \begin{matrix} 1 & 1 & k \\ J & J & J-1 \end{matrix} \right\} \left\{ \begin{matrix} 1 & 1 & k \\ I & I & I \end{matrix} \right\}.$$

The resulting equation may then be solved for Z_k , giving

$$Z_k = (2k+1) \sum_F (-1)^{I+J+F} (2F+1) \left\{ \begin{matrix} F & J & I \\ k & I & J \end{matrix} \right\} W'_F + (-1)^{2(I+J)+k} (2k+1) \left\{ \begin{matrix} 1 & 1 & k \\ J & J & J-1 \end{matrix} \right\} \left\{ \begin{matrix} 1 & 1 & k \\ I & I & I \end{matrix} \right\} \eta.$$

First, we note that this expression does not depend on the specific choice of Δ . Second, we note that for the case of $k > 2$, the triangular condition is not satisfied along the top rows of the last four six- j symbols in the last expression. Since these six- j symbols are then equal to zero, Z_k is completely defined by the values of W'_F . Equivalently, we may conclude that the HFS constants C, D, \dots may be expressed completely in terms of the HFS intervals, and these are the same expressions that would be obtained regardless of the inclusion of η . A more general proof can easily be given to show that with the inclusion of second-order dipole-quadrupole terms, C can no longer be expressed completely in terms of the intervals, while the expression for D in terms of the intervals would still remain valid (and so on to higher second-order terms if desired).

The above conclusion can also be drawn from the formulation of second-order effects as in Ref. [31], in which the second-order effects are used to describe the difference between a measured value of a HFS constant (based on first-order perturbation theory) compared to its actual value. This already assumes that all measurable HFI effects are completely described by first- and second-order perturbation theory. Further assuming that only second-order terms of the dipole-dipole type contribute to measurable effects shows that measured HFS constants differ from actual HFS constants only for the cases of constants A and B and not for higher constants.

TABLE IV: Theoretical and experimental hyperfine structure constants for the 3P_2 states of ^9Be , ^{25}Mg , and ^{43}Ca . Theoretical values include the many-body effects discussed in Section III.

| | | A , MHz | B , MHz | C/Ω , MHz/ $(\mu_N \times \text{b})$ | D/Π , MHz/ b^2 |
|------------------|--------------------|---------------|-----------|---|-----------------------------|
| ^9Be | Theory | -119.7 | 1.43 | 4.89×10^{-7} | |
| | Expt. ^a | -124.5368(17) | 1.429(8) | | |
| ^{25}Mg | Theory | -127.5 | 15.8 | 1.71×10^{-5} | -1.39×10^{-14} |
| | Expt. ^b | -128.445(5) | 16.009(5) | | |
| ^{43}Ca | Theory | -179.9 | -5.50 | 7.03×10^{-5} | 7.83×10^{-13} |
| | Expt. ^c | -171.962(2) | -5.436(8) | | |

^aRef. [28]

^bRef. [29]

^cRef. [30]

- [1] N. F. Ramsey, *Molecular beams* (Oxford University Press, London, 1969).
- [2] C. Schwartz, Phys. Rev. **105**, 173 (1957).
- [3] R. T. Daly and J. H. Holloway, Phys. Rev. **96**, 539 (1954).
- [4] H. H. Brown and J. G. King, Phys. Rev. **142**, 53 (1966).
- [5] T. G. Eck and P. Kusch, Phys. Rev. **106**, 958 (1957).
- [6] W. J. Childs, O. Poulsen, L. S. Goodman, and H. Crosswhite, Phys. Rev. A **19**, 168 (1979).
- [7] W. J. Childs, Phys. Rev. A **44**, 1523 (1993).
- [8] T. Brenner, S. Buttgenbach, W. Rupprecht, and F. Trauber, Nucl. Phys. A **440**, 407 (1985).
- [9] W. G. Jin, M. Wakasugi, T. T. Inamura, T. Murayama, T. Wakui, H. Katsuragawa, T. Ariga, T. Ishizuka, and I. Sugai, Phys. Rev. A **52**, 157 (1995).
- [10] V. Gerginov, A. Derevianko, and C. E. Tanner, Phys. Rev. Lett. **91**, 072501 (2003).
- [11] P. Raghavan, At. Data and Nucl. Data Tables **42**, 189 (1989).
- [12] S. G. Porsev and A. Derevianko, Phys. Rev. A **69**, 042506 (2004).
- [13] J. Grünert and A. Hemmerich, Phys. Rev. A **65**, 041401 (2002).
- [14] S. B. Nagel, C. E. Simien, S. Laha, P. Gupta, V. S. Ashoka, and T. C. Killian, Phys. Rev. A **67**, 011401(R) (2003).
- [15] X. Xu, T. H. Loftus, J. L. Hall, A. Gallagher, and J. Ye, J. Opt. Soc. Am. B **20**, 968 (2003).
- [16] M. Yasuda and H. Katori, Phys. Rev. Lett. **92**, 153004 (2004).
- [17] W. R. Johnson, *Atomic Structure Theory: Lectures on Atomic Physics* (Springer, New York, NY, 2007).
- [18] W. Dankwort, J. Ferch, and H. Gebauer, Z. Physik **267**, 229 (1974).
- [19] V. A. Dzuba, V. V. Flambaum, and M. Kozlov, Phys. Rev. A **54**, 3948 (1996).
- [20] I. M. Savukov and W. R. Johnson, Phys. Rev. A **65**, 042503 (2002).
- [21] W. R. Johnson, D. R. Plante, and J. Sapirstein, Adv. At. Mol. Opt. Phys. **35**, 255 (1995).
- [22] W. R. Johnson, S. A. Blundell, and J. Sapirstein, Phys. Rev. A **37**, 307 (1988).
- [23] V. M. Shabaev, I. I. Tupitsyn, V. A. Yerokhin, G. Plunien, and G. Soff, Phys. Rev. Lett. **93**, 130405 (2004).
- [24] K. Beloy and A. Derevianko, *Application of the dual-kinetic-balance sets in the relativistic many-body problem of atomic structure* (2007), arXiv:0710.3142.
- [25] B. K. Sahoo, Phys. Rev. A **73**, 062501 (2006).
- [26] S. M. Heider and G. O. Brink, Phys. Rev. A **16**, 1371 (1977).
- [27] C. Schwartz, Phys. Rev. **97**, 380 (1955).
- [28] A. Blachman and A. Lurio, Phys. Rev. **153**, 164 (1967).
- [29] A. Lurio, Phys. Rev. **126**, 1768 (1962).
- [30] P. Grundevik, M. Gustavsson, I. Lindgren, G. Olsson, L. Robertsson, A. Rosen, and S. Svanberg, Phys. Rev. Lett. **42**, 1528 (1979).
- [31] J. L. Armstrong, *Theory of the Hyperfine Structure of Free Atoms* (Wiley-Interscience, New York, 1971).